

Transport on river networks: A dynamical approach

Ilya Zaliapin ^{*}, Efi Foufoula-Georgiou [†] and Michael Ghil [‡]

November 1, 2018

Abstract

This study is motivated by problems related to environmental transport on river networks. We establish statistical properties of a flow along a directed branching network and suggest its compact parameterization. The downstream network transport is treated as a particular case of nearest-neighbor hierarchical aggregation with respect to the metric induced by the branching structure of the river network. We describe the static geometric structure of a drainage network by a tree, referred to as the *static tree*, and introduce an associated *dynamic tree* that describes the transport along the static tree. It is well known that the static branching structure of river networks can be described by *self-similar trees* (SSTs); we demonstrate that the corresponding dynamic trees are also self-similar. We report an unexpected *phase transition* in the dynamics of three river networks, one from California and two from Italy, demonstrate the universal features of this transition, and seek to interpret it in hydrological terms.

1 Introduction

The topology of river networks has been extensively studied over the past decades and stream ordering schemes, as well as statistical self-similarity concepts, have been explored to a considerable extent [see *Horton*, 1945; *Strahler*, 1957; *Shreve*, 1966; *Tokunaga*, 1978;

^{*}Department of Mathematics and Statistics, University of Nevada, Reno, USA. E-mail: zal@unr.edu.

[†]St. Anthony Falls Laboratory and Department of Civil Engineering, University of Minnesota – Twin Cities, Minneapolis, Minnesota, USA. E-mail: efi@umn.edu.

[‡]Département Terre-Atmosphère-Océan and Laboratoire de Météorologie Dynamique, Ecole Normale Supérieure, Paris, FRANCE and Department of Atmospheric and Oceanic Sciences and Institute of Geophysics and Planetary Physics, University of California Los Angeles, USA. E-mail: ghil@atmos.ucla.edu.

Mandelbrot, 1983; La Barbera and Rosso, 1987; Marani et al., 1991; Rodriguez-Iturbe et al., 1992; Peckham, 1995; Badii and Politi, 1997; Rodriguez-Iturbe and Rinaldo, 1997; Turcotte, 1997; Sposito, 1998; Peckham and Gupta, 1999; Pelletier and Turcotte, 2000; Burd et al., 2000; Dodds and Rothman, 2000; da Costa et al., 2002; and references therein]

What has been less studied, however, is how the static topology of a river network affects and is affected by the dynamical processes operating over this network. For example, consider a directed tree that represents a river network, and assume we are interested in the mixing of water, solutes and sediments as they move downstream in reaches of variable lengths and merge at junctions of the river network. One might want then to attach a “metric” to the nodes of this tree, such as the distance to the nearest source, and consider the notion of a *dynamic tree*, superimposed on the template of the underlying *static tree*.

This dynamic tree is likely to have a different hierarchy and topology than the static one. Depending on the dynamics, for example, some of the static-tree branches might be completely cut off, either due to a blockage that prevents transport along these branches or due to the absence of conditions to generate sediment or nutrient for downstream transport. In this case, the dynamic tree will have a different hierarchy than the static one, and this difference might affect the scaling of fluxes that participate in defining the envirodynamics on the network of interest. In general, a static tree of a given Horton-Strahler order could become a dynamic tree of a lesser or higher order, depending on the superimposed dynamics.

The purpose of this paper is to study the dynamic topology of directed trees, starting with several simple cases, first synthetic and then realistic. The direction we use is obviously “downstream,” *i.e.*, from the leaves to the root of the tree. We focus on a dynamic hierarchy built on the concept of “connectivity”: once two streams are connected, they both influence the downstream dynamics. One can thus imagine that two order-1 streams of different lengths, l_1 and l_2 , merge at a node but do not automatically give rise to an order-2 stream, as would be the case in the standard Horton-Strahler ordering scheme; instead, we keep track of length and the assigned order becomes 2 only when the running index of length becomes $\max(l_1, l_2)$.

Alternatively, one might keep track of time, rather than length: the two are equivalent if the flow velocity is constant along all the branches, which we will assume in the present paper, for simplicity’s sake. In other words, a dynamical node of order 2 is created only when the fluxes from both order-1 streams do reach the connecting node. Such considerations will result in a different ordering of the dynamic tree compared to the

static one. Moreover, the newly created dynamic tree will be *time-oriented*, a property that is absent in conventional static trees.

We approach the problem of hierarchical dynamics of river networks using general concepts of *hierarchical aggregation*, which studies how multiple individual particles (molecules, species, individuals, *etc.*) merge (aggregate, collide) with each other to form clusters in different physical, chemical, biological, or sociological settings. A major role in such studies is played by the notion of *cluster dynamics*. This concept refers to the situation when a system that contains an infinite number of interacting particles can be decomposed into *finite* clusters that move independently of each other for some random interval of time. After this time, the particle interactions give rise to infinite-range correlations, although the system can be decomposed into another set of finite independent clusters, and so on.

In the 1970s, Ya. G. Sinai developed a self-consistent mathematical formalism and proved the existence of cluster dynamics for some particle systems in statistical mechanics [Sinai, 1973, 1974]. The ideas of cluster dynamics have been applied to plasma physics, economics, and the study of precursory patterns for extreme events in geophysics [Rotwain *et al.*, 1997; Molchan *et al.*, 1990; Keilis-Borok and Soloviev, 2003]. Recently, Gabrielov *et al.* [2008] evaluated numerically the cluster dynamics of elastic billiards, leading to the detection of what appear to be the first genuine *phase transitions* and *scaling phenomena* that develop in time, rather than with respect to a control parameter, such as temperature T or density; *i.e.*, a transition occurs and scaling develops as time t evolves toward a critical value t^* , rather than as the parameter T crosses a critical value T^* .

In this paper, we adapt the concept of cluster dynamics to environmental transport on river networks. Notably, we obtain a remarkably similar, and equally unexpected, phase transition in the cluster dynamics of river networks and attempt to interpret it in this context. We also study the statistical properties of the dynamic trees introduced herein. It is well known that the static branching structure of river networks can be described by *self-similar trees* (SSTs); we demonstrate, using three actual river basins, that the corresponding dynamic trees are also self-similar.

This paper is structured as follows. We review in Section 2 the terms and concepts relevant to the hierarchical analysis of branching structures, including the Horton-Strahler and Tokunaga branching taxonomies. Section 3 introduces the concept of a *dynamic tree* that is associated with a given *static tree*, by using two examples from river transport. Section 4 describes two types of static trees analyzed in this study. The first type reflects the well-formed “river network” of a basin. The second type reflects the “unchannelized

drainage network”; this network is composed of drainage paths that are not permanent channels but are perpendicular to the topographic contour lines and follow the steepest downstream gradient. In other words, this drainage network is formed by paths of “zero-order” basins or hillslopes. Hierarchical aggregation is described in greater depth, and with additional examples from several fields, in Section 4, along with an abstract metric space setup. Three actual river networks, from California and Italy, are analyzed in Section 6. A summary and discussion follow in Section 7.

2 Main concepts and definitions

This section introduces the main concepts used in the analysis of branching structures, along with their definitions and illustrative examples.

2.1 Trees

A *tree* \mathbb{T} is a set of *nodes* connected by *vertices* (also called *edges* or *links*) in such a way that there are no loops, *i.e.* there are no closed paths formed by distinct edges (see Fig. 1). A *rooted tree* has one special node designated as a *root*. In a rooted tree each connected pair of nodes has a parent-child relationship, with the parent being the element that is closest to the root [Athreya and Ney, 1972]. The nodes with no children are called *leaves*. The *depth* d_i of a node i in a rooted tree is defined as the number of edges between this node and the root. The depth D of a tree is the maximum of the depths d_l over all the leaves l .

In this study we will work with *binary trees*. In a binary rooted tree, each node may have either two or no children. This means that each internal node i (every node except for the root and the leaves) is connected to three other nodes: one is a parent of i , and the other two are its children. The root is only connected to two children, and each leaf is connected to a single parent. A *complete binary tree* is a rooted tree such that all its leaves have the same depth. Our interest for binary trees is motivated by the observation that many natural phenomena exhibit binary branching. For example, in river networks, it is unlikely for three or more streams to merge at exactly the same point, while in gas dynamics it is unlikely that more than two molecules will collide at the same time.

In our study of river transport, the tree \mathbb{T} will represent a drainage network; see Fig. 1. Hence the nodes correspond to the merging points of streams and vertices to the stream segments between these points, while the network’s sources are the leaves, and

the outlet is the root of the tree.

2.2 Branching-order taxonomies

In many applications, there is a need to order the nodes according to their importance in forming the entire hierarchy; this importance often corresponds also to relative size. For instance, in a botanical tree the leaves are the most delicate, smallest elements; the intermediate levels are formed by consecutively wider branches, while the most heavy, robust element of the plant is its trunk. Likewise, one naturally distinguishes in a river network between minor and major tributaries, according to the amount of water that they are able to carry.

In a complete tree, the node ordering task is quite straightforward since a node’s order can be chosen to be inversely proportional to its depth: “the deeper, the smaller”. The problem, however, becomes more complicated when one deals with an incomplete tree; in this case, the depth can no longer serve as a proxy for size, since the leaves, while being the smallest elements, will often be assigned indices that are as large as those of much heavier internal nodes.

Horton [1945] developed a convenient way to order hierarchically organized river tributaries; this method was later refined by *Strahler* [1957] and further expanded by *Tokunaga* [1978]. Currently, the so-called Horton-Strahler and Tokunaga ordering schemes are standard tools of branching analysis.

2.2.1 Horton-Strahler ordering

Each leaf in a binary rooted tree is assigned a Horton-Strahler (HS) *order* $r(\text{leaf}) = 1$; see Fig. 2a. Each node p , which is the parent of nodes c_1 and c_2 , is assigned a Horton-Strahler order $r(p)$ according to the following rule [*Horton*, 1945; *Strahler*, 1957; *Newman et al.*, 1997]:

$$r(p) = \begin{cases} r(c_1) + 1 & \text{if } r(c_1) = r(c_2) \\ \max(r(c_1), r(c_2)) & \text{if } r(c_1) \neq r(c_2). \end{cases} \quad (1)$$

A *branch* is defined as a union of connected nodes with the same order. We will denote by N_r the total number of branches of order r . Notice that each branch has *linear* structure: two children of the same parent can not belong to the same branch.

In a tree with n leaves, the longest branch can be formed by $(n - 1)$ nodes; this is the case when two leaves merge together to form an order-2 branch and then all other leaves join this branch one by one. We refer to this situation as *exhaustive branching*. It

is readily seen that each leaf is always an order-1 branch. An order-2 branch is created by merging two leaves and can consist of more than one node, depending on the leaves that join it; an order-2 branch that consists of two nodes is highlighted in Fig. 2a. The order Ω of a tree is the maximal order of its branches (or nodes).

In a complete tree, each branch consists of a single node since the children of an order- r node always have the same order ($r - 1$). In such a tree, the HS order is uniquely determined by the node depth d via $r = D - d + 1$, where the tree depth is $D = \Omega$.

2.2.2 Tokunaga indexing

Tokunaga indexing [Tokunaga, 1978; Peckham, 1995; Newman et al., 1997] extends upon the Horton-Strahler orders; it is illustrated in Fig. 2b. This indexing focuses on incomplete trees by cataloging the merging points between branches of different order. A first-order branch that merges with a second-order branch is indexed by “12” and the total number of such branches is denoted by N_{12} . A first-order branch that merges with a third-order branch is indexed by “13” and the total number of such branches is N_{13} , and so on. In general, N_{ij} for $j > i$ denotes the total number of order- i branches that join an order- j branch.

The Tokunaga index T_{ij} is the number of branches of order i that merge with a branch of order j , normalized by the total number of branches of order j ; in other words, T_{ij} is the average number of branches of order $i < j$ per branch of order j :

$$T_{ij} = \frac{N_{ij}}{N_j}. \quad (2)$$

Merging of branches of different orders is referred to as *side branching*. It is easily seen that side branching is absent in a complete tree, and “a tree with side branching” is synonymous to “an incomplete tree.” For incomplete trees, the side-branching indices become increasingly important as they help to define a tree’s structure, possibly indicating properties that are unique to specific classes of trees.

For consistency, we denote the total number of order- i branches that merge with other order- i branches by N_{ii} and notice that in a complete binary tree $N_{ii} = 2 N_{i+1}$. This allows us to formally introduce the additional Tokunaga indices:

$$T_{ii} = \frac{N_{ii}}{N_{i+1}} \equiv 2.$$

The set $\{T_{ij} : 1 \leq i, j \leq \Omega\}$ of Tokunaga indices provides a complete statistical description of the branching structure of an order- Ω tree.

2.2.3 Other node statistics

We introduce here two node statistics relevant to our river transport study:

- the *number of nodes* (or links) within a branch i is denoted by c_i ; and
- the *magnitude* m_i of a node i is the number of leaves that descend from i ; in other words, the magnitude of a branch is the number of the sources upstream of it.

Magnitude measures the complexity of the river structure upstream from a given branch. We notice that each leaf (source) has unit magnitude, $m_{\text{leaf}} = 1$, and the magnitude of a parental node p is the sum of the magnitudes of its children c_1 and c_2 :

$$m_p = m_{c_1} + m_{c_2}. \quad (3)$$

Accordingly, a node of order r has magnitude $m \geq 2^{r-1}$, with equality being attained only for a complete binary tree. The average number of nodes and average magnitude of an order- r branch are denoted by C_r and M_r respectively.

2.3 Self-similar trees

The concept of *self-similarity* provides a powerful tool for describing and studying trees. A self-similar tree (SST) is defined by the constraint

$$T_{i,i+k} = T_k \quad \text{for } k = 1, 2, \dots \quad (4)$$

E. Tokunaga was probably the first to study SSTs, and considered an additional constraint on the branching indices [Tokunaga, 1978]:

$$\frac{T_{k+1}}{T_k} = c, \quad \text{or} \quad T_k = a c^{k-1} \quad \text{for } a, c > 0. \quad (5)$$

The SSTs that satisfy (5) are called *Tokunaga trees*.

2.4 Horton laws

Empirically, the average values of branching statistics for the observed river basins depend exponentially on the order r :

$$N_r = N_0 R_B^{\Omega-r}, \quad (6)$$

$$M_r = R_M^{r-1}, \quad (7)$$

$$C_r = C_0 R_C^r \quad (8)$$

for some positive constants N_0 and C_0 . Such relationships are called *Horton laws*; the bases R_B, R_M , and R_C of the exponential relationships are called *stream ratios*.

McConnell and Gupta [2008] showed that the Horton laws (6), (7) hold asymptotically, *i.e.* for $r \rightarrow \infty$, in a self-similar Tokunaga tree; they also proved that $R_B = R_M$. Moreover, *Zaliapin* [2009] demonstrated the stream ratio inequality

$$R_B = R_M < R_C, \tag{9}$$

that had been conjectured by *Peckham* [1995]. In addition, *Zaliapin* [2009] demonstrated that the Horton laws hold, under some additional assumptions on the Tokunaga indices T_k , for self-similar trees that do not necessarily satisfy the Tokunaga condition (5).

3 Static vs. dynamic trees: Network envirodynamics

The topological structure of a river network is well described by a tree, which we denote by \mathbb{T}_S and call the *static tree*. To describe the downstream transport on \mathbb{T}_S we now introduce a *dynamic tree* \mathbb{T}_D , which can be interpreted as follows. Imagine that we inject a dye simultaneously into all the sources of our river network, represented by the leaves of \mathbb{T}_S , and the dye starts propagating down the river, from the sources to the outlet, with the same constant velocity along all the streams. The tree \mathbb{T}_D describes the time-dependent history of the mergings of the colored streams.

Next, we consider two detailed examples that will clarify this important concept. We restrict ourselves to the simplest case of constant velocity along all the streams; taking this velocity to be unity, time and length scales can be interchanged. An extension to spatially or temporally variable velocities is straightforward: we shall see that the dynamic tree \mathbb{T}_D is completely determined by the static tree \mathbb{T}_S and the set of time *delays* τ_i necessary for the dye to propagate from a node i to its parent.

3.1 Synthetic example

Figure 3 shows how to construct the dynamic tree for a basin with four sources **a**, **b**, **c**, and **d**. The static tree for this basin is a complete binary tree shown in the top right panel. The same tree with the link lengths explicitly shown is placed in the top row of panels; the top left panel indicates the values of these lengths.

The consecutive phases of construction of the dynamic tree are shown in the bottom row of panels. At step 0 (the leftmost top and bottom panels), all the links in the tree are “empty” (dashed lines) and the dye is injected into the sources **a**, **b**, **c**, and **d**. Accordingly, we have four disconnected clusters of colored flux; they correspond to four disconnected nodes in the lower left panel. Each step in the figure is a snapshot of the process after a unit time interval; recall that we only use constant velocity in this paper and, without loss of generality, this velocity equals unity.

At step 1 the dye has propagated a unit length along each stream, which is depicted by solid lines in the top panel. Since all four streams are disconnected so far, the dynamic tree still consists of four disconnected branches, each of which corresponds to a colored stream of unit length. At step 2 the streams **a** and **b** merge. This is reflected in the dynamic tree, where the nodes **a** and **b** are now connected into a single cluster. Notice that the leaves **a** and **b** are not directly connected in the static tree; this connection reflects a special property of the dye’s downstream propagation.

At step 3 stream **c** reaches stream **a**. Since stream **a** by that time is already merged with stream **b**, we say that the stream **c** merges with the cluster of **a** and **b**; this is reflected in the dynamic tree in the lower panel for this step. Hence, at step 3 there exist two connected clusters of the colored flux: one cluster is formed by the streams **a**, **b**, and **c**, while stream **d** alone forms the second cluster. Finally, at step 4, all the colored fluxes merge together. The conventional representation of both static and dynamic trees, which does not show the link lengths, is given in the two rightmost panels.

This example shows that the dynamic tree \mathbb{T}_D can be very different from the corresponding static tree \mathbb{T}_S . We notice in particular that in this example the static tree is a tree with no side branching; it has the largest possible Horton-Strahler order, $\Omega = 3$, for a tree with four leaves. At the same time, the dynamic tree exhibits exhaustive side-branching; accordingly, it has the smallest possible order, $\Omega = 2$, for a four-leaved tree.

3.2 Realistic example

Here we illustrate the dynamic tree for an order-3 subbasin of the Noyo basin; this basin is located in Mendocino County, California, USA, and is described by *Sklar et al.* [2006]. The stream network for this subbasin is shown in Fig. 4; its fifteen sources are marked by numbers 1 to 15 and fourteen stream joints by letters **a** to **n**. The static tree \mathbb{T}_S for this stream network is shown in Fig. 5a; it has the Horton-Strahler order $\Omega = 3$.

The time-oriented dynamic tree \mathbb{T}_D is shown in Fig. 5b against the time axis (on the

ordinate); notice that time can also be interpreted as the distance traveled by the dye from each source. This interpretation has a direct connection to the metric properties of the basin and we will use it in the subsequent analysis. The order of the dynamic tree is $\Omega = 4$. The letter and number marks in Fig. 5 match those in Fig. 4.

Four snapshots of the dye propagation — at times $t = 1, 20, 39$, and 60 — are shown in Fig. 6. In this example, the dynamic tree shows a larger degree of side-branching compared to the static tree; this larger degree is reflected in its larger HS order. We shall see in other realistic examples, further below, that this seems to be the case for most actual river networks.

4 Stream vs. hillslope networks

In an actual landscape, channels are initiated when the area upstream suffices to create a sustainable source of streamflow and this source imprints a permanent channel on the terrain. Although these channels are typically detectable by field observations, the extraction of the channel initiation points, or “channel heads,” from Digital Elevation Models (DEMs) has been a subject of intense study. Most commonly, channels are assumed to be initiated when the upstream area, or area times a typical slope, exceed a given threshold; the parameters of such relationships are field-calibrated. More recently, the availability of high-resolution, 1-m elevation data from LIght Detection and Ranging (LIDAR) instrumentation has initiated a new generation of methodologies for the automatic detection of channels as “edges” or “features” in the terrain [*e.g.*, *Lashermes et al.*, 2007; *Passalacqua et al.*, 2009].

The channelized paths, *i.e.* the branches of the river network, are not the only parts of the basin by which water or other fluxes — *e.g.*, sediments, nutrients, or pollutants — are transported downstream. The unchannelized part of the basin, often called *zero-order basins* or *hillslopes*, is drained by pathways that have their own topology. In this work, we extract (i) *stream networks* from DEMs by using a critical threshold area A_c , and (ii) *hillslope networks* by assuming that A_c is as small as the DEM resolution.

Clearly, each stream network is a part of the corresponding hillslope network. For a generic river basin, though, the total length of channelized paths is much smaller than the total length of unchannelized paths. In the present study, we assume that stream networks reflect the properties of channelized paths, while hillslope networks reflect the properties of unchannelized paths. The study of unchannelized-path topology below will show that it is quite different from the topology of the channelized paths.

Construction of stream and hillslope static trees is illustrated in Fig. 7. Figure 7a shows a small part of a river basin; it is divided into 16 square regions called *pixels*. The well-defined streams occupy some of the pixels (shaded squares), the rest of the pixels (white squares) represent *hillslopes*, *i.e.* unchannelized parts of the basin.

The elevation data can be used to figure out the flux direction from each pixel, whether stream or hillslope; this direction is depicted by arrows in Fig. 7b. We assume that there is a unique flux direction away from each pixel; at the same time, fluxes can reach a given pixel from more than one other pixel. This property allows one to represent the directional information by a tree, which is shown in Fig. 7c. Solid nodes and solid lines in the figure represent the stream pixels and the stream flow respectively, while open nodes and dashed lines represent the hillslope nodes and hillslope flow.

The final step in creating the static tree of this subbasin is to remove the linear segments (chains), that is to remove the nodes with only two connections (except the tree root). The resulting static hillslope tree is shown in panel (d). The static stream tree is obtained from the hillslope tree by removing the dashed links that represent unchannelized paths, and removing the remaining chains; the stream tree for our example is shown in panel (e).

5 The dynamics of hierarchical aggregation

The consecutive merging of river streams discussed in the previous section is a special case of a general phenomenon of *hierarchical aggregation*. This phenomenon is also called *inverse cascading*, and it can be described as follows.

Consider a process that starts at time $t = 0$ with N individual *particles*, which can be considered as *clusters* of unit mass. As time evolves, the clusters start to merge with one another, according to a set of suitable rules, thus forming consecutively larger clusters. We assume that only two clusters can merge at the same time; thus after each merging the number of clusters decreases by one. The process continues until all particles have been merged into a single cluster of mass N . The evolution of the above process can be described by a time-oriented binary tree, whose leaves correspond to the initial particles, the root to the final cluster of N particles, and each internal node to the merging of a particular pair of clusters.

5.1 Examples

Among the many instances of the above general aggregation scheme, we mention here the following four.

Percolation. In the *site percolation* process on an $L \times L$ lattice, the initial $N = L^2$ particles correspond to the sites of the lattice, while clusters correspond to connected patches of occupied sites that are formed during the percolation process [Zaliapin *et al.*, 2005]. In fact, the same scheme can be applied to bond percolation, as well as to percolation on grids in higher dimensions.

Billiards. *Elastic billiard* on a rectangular table can be used to model *gas dynamics* in two dimensions (2-D). Here the initial particles are the N billiard balls (gas molecules) at time $t = 0$. Each of the balls is assigned an initial position and velocity. The clusters at time Δ are formed by balls that have collided during the time interval $[0, \Delta]$ [Gabrielov *et al.*, 2008]. Formally, two balls are called Δ -neighbors if they collided during the time interval $[0, \Delta]$. Each connected component of this neighbor relation is called a Δ -cluster. Notice that within an arbitrary Δ -cluster each ball has collided with at least one other ball during the time interval $[0, \Delta]$. In other words, a Δ -cluster is a group of balls that have affected each other's dynamics during the time interval of duration Δ . The mass of each cluster is simply the total number of balls within that cluster. Upon many collisions of the balls, the whole system will be composed of clusters of different sizes. As time evolves, the number of clusters will decrease and their mass increase.

The same scheme can be applied to a system of particles that interact according to some potential $U(\mathbf{x})$. Bogolyubov [1960] suggested that when the interaction of particles is short-ranged, the system can be decomposed into finite clusters so that during some random interval of time, each cluster moves independently of other clusters as a finite-dimensional dynamical system. After this time interval, the system can be decomposed again into other dynamically independent clusters and so on. This type of dynamics is called *cluster dynamics* and Sinai [1974] showed analytically that it exists in a one-dimensional (1-D) system of statistical mechanics. Numerical results of Gabrielov *et al.* [2008] describe the presence and various properties of cluster dynamics in a 2-D system of hard balls.

Phylogenetic trees. Probably the best-known application of hierarchical aggregation is in constructing phylogenetic trees that describe the evolutionary relationships among

biological species [Maher, 2002]. Here, a node corresponds to a set of species. Two species are connected if they have a direct common ancestor; the link length from a species to its direct ancestor equals the time it took to develop the descendant species from that ancestor.

River transport. The example of interest to us here is the downstream transport along a river network. In this case, the initial particles are the environmental fluxes at the sources of the network, and clusters are formed by consecutive merging of the streams down the river path. That is, new clusters are formed when fluxes from upstream merge at the stream junctions. This scheme of describing dynamics along a static tree was considered in detail in Section 3, albeit without referring to hierarchical aggregation.

5.2 General set-up

Hierarchical aggregation can be described in great generality by using the framework of nearest-neighbor clustering in a metric space. Specifically, consider a set \mathbb{S} with distance $d(a, b)$ for $a, b \in \mathbb{S}$; the elements of the set will be called *points*. The distance $d(A, B)$ between two subsets of points $A = \{a_i\}_{i=1, \dots, N_A}$ and $B = \{b_i\}_{i=1, \dots, N_B}$ from \mathbb{S} is defined as the shortest distance between the elements of the sets:

$$d(A, B) = \min_{1 \leq i \leq N_A, 1 \leq j \leq N_B} d(a_i, b_j).$$

Nearest-neighbor clustering is a process that combines points from \mathbb{S} into consecutively larger subsets, called *clusters*, by connecting at each step the two nearest clusters; this process can be described by the *nearest-neighbor spanning tree* \mathbb{T} . Specifically, consider N points $c_i^0 \in \mathbb{S}$, $i = 1, \dots, N$ with pairwise distances $d_{ij}^0 \equiv d(c_i^0, c_j^0)$. These points, considered as clusters of unit mass ($m_i = 1$), form N leaves of the time-oriented tree \mathbb{T} . The first internal tree node is formed at the time $t_1 = \min_{ij} d_{ij}^0$ by merging two closest points $c_{i^*}^0$ and $c_{j^*}^0$ with $(i^*, j^*) = \operatorname{argmin}_{ij} d_{ij}^0$, where $\operatorname{argmin}_{ij} f(i, j)$ is defined as a pair (i^*, j^*) such that $f(i^*, j^*) = \min_{ij} f(i, j)$. This merging creates a new cluster of two points, with a mass of $m_i + m_j = 2$. Hence, at time t_1 , there exist $N - 1$ clusters: $N - 2$ clusters with unit mass and one cluster of mass $m = 2$.

We can now reindex the clusters so as to work with clusters c_i^1 , $i = 1, \dots, N - 1$; their total mass is $\sum_{i=1}^{N-1} m_i = N$ and pairwise distances are $d_{ij}^1 \equiv d(c_i^1, c_j^1)$. The second internal node of tree \mathbb{T} is formed at time $t_2 = \min_{ij} d_{ij}^1 > t_1$ by merging the two closest clusters from the set $\{c_i^1\}_{i=1, \dots, N-1}$. Thus, at time t_2 we have $N - 2$ clusters c_i^2 such

that their total mass is N and pairwise distances are $d_{ij}^2 \equiv d(c_i^2, c_j^2)$. We continue in the same fashion, so the k -th internal cluster, for $1 \leq k \leq N - 2$, is formed at time $t_k = \min_{ij} d_{ij}^k > t_{k-1}$, and at that time we have $(N - k)$ clusters c_i^k , $i = 1, \dots, N - k$ with masses m_i such that $\sum_{i=1}^{N-k} m_i = N$. Finally, at time t_{N-1} we create a single cluster of mass N that combines all points c_i^0 ; this cluster forms the root of the tree \mathbb{T} .

Consider two nodes a and b from the nearest-neighbor tree and let t_a and t_b be their time marks; recall that the tree is time-oriented by the definition of the successive times $t_k = \min_{ij} d_{ij}^k > t_{k-1}$ at which the cluster mergers occur. The *ancestors* of a node are its parent, the parent of that parent, and so on, all the way to the root. Clearly, the time mark for an ancestor is larger than that of a descendant. The *nearest common ancestor* p of nodes a and b is their common ancestor with the minimal time mark t_p .

The distance $u(a, b)$ along the the nearest-neighbor tree is defined as the maximum of the values $u(a, p) \equiv t_p - t_a$ and $u(b, p) \equiv t_p - t_b$. This distance satisfies two of the usual distance axioms, symmetry and strict positivity, but the triangle inequality can be replaced by a more stringent one, namely

$$u(a, b) \leq \max[u(a, c), u(c, b)],$$

which holds for any three nodes a, b and c . Such a distance function is called an *ultrametric* [Rammal et al., 1986; Schikhof, 2007]. Ultrametric spaces have many peculiar properties; for instance, one can rename *any* triplet a, b, c of nodes in such a way that

$$u(a, c) = u(b, c).$$

These unusual properties give ultrametric spaces considerable flexibility in applications, and point sets connected via nearest-neighbor clustering are a representative example of such spaces.

In the billiard example of Section 5.1, the space \mathbb{S} is the set of N billiard balls and the ultrametric distance function $u(a, b)$ equals the time before the first collision of the balls a and b . Naturally, their distance depends on the initial positions and velocities of the two balls a and b , but it is affected by the global billiard dynamics: our two balls may be set to collide at a given time t^* in the absence of other balls, but may be hit by some other ball at time $t < t^*$, thus postponing the collision of a with b .

In our river transport problem, the space \mathbb{S} is the set of all river sources. The ultrametric distance $u(a, b)$ between two sources is defined as the time necessary for the corresponding fluxes injected into these two sources to meet down the river path. If the static river geometry is described by the tree $\mathbb{T}_{\mathbb{S}}$ — and we assume, as previously stated,

that fluxes move with unit speed downstream — the traditional distance $d(a, b)$ between two sources equals the maximal length along the tree to their nearest common parent in \mathbb{T}_S . The nearest-neighbor spanning tree of hierarchical-aggregation theory becomes what we called so far, in the context of river transport, the dynamic tree \mathbb{T}_D . As previously stated, this dynamic tree differs, in general, from the static tree \mathbb{T}_S and depends not only on the topology of the latter, but also on the actual length of the links. If the velocities vary in time or space, then the spanning tree \mathbb{T}_D will depend on the specific dynamics of the processes operating on the static tree.

To better understand transport on river networks, we will elucidate in the next section the connection between the statistical properties of \mathbb{T}_S and those of \mathbb{T}_D .

6 Analysis of drainage networks

In this section we quantify similarities and differences between the branching topology of static and dynamic trees, both at the stream and hillslope network scale.

6.1 Data description

We have analyzed three river basins: Upper Noyo (Mendocino County, California, USA), Tirso (Sardinia, Italy), and Grigno (Trento, Italy). Information about the physiographic and geologic characteristics of these basins can be found in, respectively, *Sklar et al.* [2006], *Pinna et al.* [2004], and *Guzzetti et al.* [2005]. The available DEMs were at a resolution of $10 \times 10 \text{ m}^2$ for the Noyo basin, $30 \times 30 \text{ m}^2$ for the Grigno basin, and $100 \times 100 \text{ m}^2$ for the Tirso basin. Since the focus of this study is not the extraction of the most accurate river network from the available DEMs, we felt comfortable adopting a simple criterion for channel initiation as 100 pixels for all basins. Our main conclusions about the comparison between the static and dynamic trees would not be affected by changing the critical threshold areas within reasonable ranges.

The static trees we extracted from these DEMs for the three stream networks are shown in Fig. 8. Using the procedure described earlier, we also extracted the static trees for the hillslope networks, which drain every pixel of a basin, by using a steepest gradient algorithm. The corresponding dynamic stream and hillslope trees were then constructed for each basin, assuming a constant unit speed of downstream propagation for the fluxes. Thus, we analyzed four different kinds of tree — static stream, dynamic stream, static hillslope, and dynamic hillslope — for each basin.

6.2 Self-similar properties

Figures 9 and 10 show the distributions of the number N_r , average magnitude M_r , and the average number C_r of links for branches of order r . The results in Fig. 9 refer to the stream trees; the results in Fig. 10 to the hillslope trees.

Despite the small-sample fluctuations, the figures demonstrate a large degree of consistency among the branching indices for the trees from different classes. All considered branching statistics are closely approximated by the Horton laws. Moreover, the results suggest that the relationship (9) holds in all the considered cases. Furthermore, we observe that the values of the stream ratios for static trees are higher than the corresponding values for dynamic trees; and the values of the stream ratios for stream trees are smaller than the corresponding values for hillslope trees.

The only indices that considerably deviate from the Horton laws at higher orders are C_r (average number of nodes within an order- r branch) for the Noyo basin and this warrants special investigation in the future. Apart from this discrepancy, overall we conclude that the four classes of trees, dynamic vs. static and stream vs. hillslope, can be closely approximated by the Tokunaga SSTs.

6.3 Phase transition in hierarchical dynamics

Here we ask the question as to whether the river network connectivity (in terms of elements of the network participating in transport) exhibits a *phase transition* akin to those found in other systems. Figure 11 shows the fractional magnitudes m_i/N of the branches in the dynamic trees (stream and hillslope trees of the three river basins) as a function of the distance d traveled by the dye. Recall that this distance can also be interpreted as the time t when the node was created by merging of upstream branches. Altogether we consider six cases; in all of them one observes the following scenario. We start at distance $d = 0$ (or time $t = 0$) with N branches (clusters) of unit magnitude corresponding to the most outer nodes of the transport tree. As distance increases (time evolves), the number of clusters decreases while their magnitudes become larger and exhibit prominent variability. In particular, at the small distances the maximal magnitude increases exponentially with distance; this is reflected by an approximately linear form of an upper envelop of the points in the figures (the envelop is not shown). Furthermore, we notice that at the small distances (times) the magnitude distribution is “continuous” in a sense that it does not have significant gaps. However, at some critical time t^* (translated here to distance d^* for easier interpretation), the distribution undergoes a serious qualitative

change: a prominent maximal cluster appears, such that its magnitude becomes significantly larger than that of the second larger cluster. Moreover, while the magnitude of the largest cluster keeps growing, the rest of the distribution is fading off so after some time all clusters present at $d = 0$ merge with the largest cluster. An interesting observation is that at the critical distance d^* the magnitude of the largest cluster is just about 10% of the total magnitude N of the system. Notably, this number is universal for all the considered examples.

Figure 12 shows the magnitude distribution of the clusters that existed when the dye traveled a given distance d . The analysis is done for the critical distance d^* and a smaller distance $d \approx d^*/2$; they are both indicated by vertical lines in Fig. 11. In all six cases, we see that the magnitude distribution at the smaller distance (squares) has an exponential tail, while at the critical distance (circles) it is a power law. Recall that, in a log-log plot, power-law behavior shows up as a straight line, while exponential behavior becomes a convex curve. This change indicates that a phase transition occurs at the distance d^* .

This phase transition is further illustrated in Fig. 13, which shows three snapshots of the dye propagating down the Noyo basin. The distances traveled by the dye at these snapshots are marked by vertical lines in Fig. 14; the figure shows the number of clusters (dotted line) and the magnitude of the largest cluster for the Noyo dynamic tree (solid line), as a function of downstream propagation distance.

The values of the six critical distances d^* shown in Fig. 11 vary over two orders of magnitude and depend strongly on the particular network being analyzed. Nevertheless, we notice a very good power-law fit for the value of d^* in terms of the average link length \bar{L} of the corresponding static tree (see Fig. 15):

$$d^* \approx 3.5 \bar{L}. \quad (10)$$

This relationship can be interpreted as follows in terms of the transport on river networks: the giant cluster of connected streams is formed when each flux traveled approximately 3.5 links downstream from a source. We conjecture that: (a) this is a universal property of downstream transport on Tokunaga trees with rich branching, *i.e.* Tokunaga SSTs with $c > 1$ in Eq. (5); (b) the coefficient of proportionality in (10) may depend on the Tokunaga parameters, but only weakly; and (c) this coefficient is larger than or equal to 2 for *any* binary tree. An in-depth investigation of this issue is left for future study.

7 Concluding remarks

7.1 Summary

This study focused on the statistical description of environmental transport on self-similar river networks. We approached the problem by considering downstream transport on such a network as a particular case of nearest-neighbor *hierarchical aggregation*; the so-called *ultrametric* induced by the branching structure of the river network provides the distance function with respect to which the downstream flow gives rise to clusters that decrease in number and increase in size with time.

We described the static topological structure of a drainage network by the type of tree structure that goes back to the pioneering studies of *Horton* (1945), *Strahler* (1957) and *Shreve* (1966), and referred to it as a *static tree*, to distinguish it from the associated *dynamic tree*. This novel concept introduced herein describes downstream transport along the static tree.

We studied the statistical properties of both static and dynamic trees using the Horton-Strahler (HS) and Tokunaga branching taxonomies [see *Horton*, 1945; *Strahler*, 1957; *Tokunaga*, 1978]. Using three river networks — the Noyo, Grigno and Tirso — we showed that both static and dynamics trees can be well approximated by Tokunaga *self-similar trees (SSTs)*. The HS and Tokunaga parameters of these two types of trees differ significantly, though, for each of the three basins. This difference supports the relevance of the dynamic tree concept; its parameter values depict important properties of the transport on a given river network that are not captured by the conventional, static tree.

A striking result of this study is the phase transition we found in river network dynamics: as one fills an empty river network through its sources, or injects a dye into a water-filled one, the number of clusters of connected nodes decreases and the size of the largest cluster increases, until a dominant cluster of connected streams forms. During this process, the time-dependent size distribution of the connected clusters changes from an exponential to a power-law function as the critical time approaches.

This phenomenon, which may seem rather unexpected in the present, hydrological setting, can be better understood within the framework of complex networks. This framework has been explored in many natural and socio-economic settings, ranging from the functioning of a cell to the organization of the internet [*Albert and Barabasi*, 2002].

The mathematical theory of complex networks considers a group of nodes that can be connected with each other according to some problem-specific rules, thus forming a

graph. In the simplest case, the node connections are independent of each other and can be specified by the probability p that two randomly chosen nodes are connected. There exists a critical value p_c such that for $p < p_c$ the network consists of isolated clusters, while a single giant cluster appears as p crosses p_c , and spans the entire network. The appearance of this giant cluster is remarkably reminiscent of infinite-cluster formation in percolation theory [Stauffer and Aharony, 1994]. Albert and Barabasi [2002] provide a comprehensive review of parallels and differences between complex-network theory and percolation theory.

It readily follows from the analysis of Section 3 that the transport on river basins fits rather naturally the complex-network paradigm. Formally, each river source is represented by a node and two streams are considered to be connected when their respective fluxes join downstream. This is exactly the scheme we used to define a dynamic tree, with the only difference that we ignored the node connections within already formed clusters. This difference does not affect the process of cluster formation, so all the results of complex-network theory do apply to the envirodynamics of river basins.

There is an important difference, though, between complex networks in general and the dynamic trees considered in this study. Our dynamic trees, unlike general networks, are time-oriented, *i.e.*, their nodes can be ordered according in “time” or with respect to a “distance” parameter. The ultrametric distance along such trees satisfies a stronger triangle inequality than ordinary distance (see Section 5.2). Spaces equipped with an ultrametric u , instead of a traditional distance d , have therefore interesting properties [*e.g.*, Schikhof, 2007]. As shown in Section 5, hierarchical aggregation via nearest-neighbor clustering provides a common framework for many apparently different processes — *e.g.*, billiards, river transport, and percolation — in the setting of ultrametric trees, and thus may provide novel insights into these processes.

In percolation models, the cluster-size distribution at phase transition is given by a power law, whose index is a function of the system’s dimension alone. In our three river networks, this index differs from the one to the other, and from the river to the hillslope network for the same basin. In our hierarchical aggregation on dynamic trees, different clustering rules may correspond to different effective “dimensions” of the system. At the same time, it is known that the critical percolation indices are universal for systems in high dimensions [Hara and Slade, 1990] and trees are a simple model for infinite-dimensional systems [Albert and Barabasi, 2002]. Thus, one expects to see the same values of the critical indices when working with percolation on a tree. From this perspective, the fact that our critical exponents vary from basin to basin, and from river to hillslope

trees, still needs to be understood.

7.2 Discussion and further work

In this study we considered only the simplest clustering rules for the river streams: two streams belong to the same cluster if there is a connected path from one stream to another along the river network. This approach is patterned after percolation studies and allows for a straightforward treatment. It might however result in a situation when two streams belong to the same cluster despite the fact that the respective fluxes are not mixed yet (think of two short streams that merge with a spatially extended cluster at about the same time). Formulating a physically more appropriate set of clustering rules might yield more realistic results for a wealth of river networks with differing properties.

So far, we only investigated dynamic trees that have the same set of leaves as the corresponding static tree; this corresponds to injecting a flux through the sources. At the same time, it might happen that a flux of interest is injected into an internal node, *e. g.*, an industrial pollutant from a plant or nutrient production from a local biotic activity. Such situations can be easily modeled by considering a dynamic tree whose set of leaves samples the entire river network.

To construct a richer theoretical framework for transport on river networks one may also model the transport along real and synthetic networks by using Boolean delay equations (BDEs). In BDEs, the discrete state variables describe the flux through the river branches; naturally, the rules for updating these variables inherit the child-parent relationship of the stream's static tree. The parent variables are updated based on the values of the children variables, after delays that correspond to time of flux propagation from a child to its parent. *Ghil et al.* [2008] reviewed recently BDEs and their applications to climate and earthquake modeling. We expect such modeling to shed further light on the complex and important problems of river transport.

8 Acknowledgements

This research was supported by the National Center for Earth-surface Dynamics (NCED), a Science and Technology Center funded by NSF under agreement EAR-0120914, as well as by NSF grants EAR-0824084 and EAR-0835789. We thank Paola Passalacqua for helping with the river network extraction.

References

- [1] Albert, R. and A.-L. Barabasi (2002), Statistical mechanics of complex networks, *Rev. Mod. Phys.* *74*, 47-97.
- [2] Badii, R. and A. Politi (1997), *Complexity: Hierarchical Structures and Scaling in Physics*, Cambridge University Press, 318 pp.
- [3] La Barbera, P. and R. Rosso (1987), Fractal geometry of river networks, *EOS Trans. AGU*, *68(44)*, 1276.
- [4] Blanter, E. M., M. G. Shnirman, J. L. LeMouel, and C. J. Allegre (1997), Scaling laws in blocks dynamics and dynamic self-organized criticality, *Phys. Earth Planet. Inter.*, *99(3-4)*, 295-307.
- [5] Blanter, E. M., M. G. Shnirman, and J. L. LeMouel (1997), Hierarchical model of seismicity: scaling and predictability, *Phys. Earth Planet. Inter.*, *103(1-2)*, 135-150.
- [6] Boltzmann, L. (1896), *Vorlesungen über Gastheorie*, Bands I, II.
- [7] Bogolyubov, N. N. (1960), *Problems of Dynamic Theory in Statistical Physics*, Oak Ridge, Tenn., Technical Information Service.
- [8] Burd, G. A., E. C. Waymire, and R. D. Winn (2000), A self-similar invariance of critical binary galton-watson trees. *Bernoulli*, *6(1)*, 1-21.
- [9] da Costa, F. P., Grinfeld, M., Wattis, J. A. D. (2002), A hierarchical cluster system based on Horton-Strahler rules for river networks, *Studies Appl. Math.*, *109(3)*, 163-204.
- [10] Dodds, P.S. and D.H. Rothman (2000), Scaling, Universality, and Geomorphology, *Annual Review of Earth and Planetary Sciences*, *28*, 571-610, doi:10.1146/annurev.earth.28.1.571.
- [11] Gabrielov, A. M., V. I. Keilis-Borok, I. V. Zaliapin, and W. I. Newman (2000a), Critical transitions in colliding cascades, *Phys. Rev. E*, *62*, 237-249.
- [12] Gabrielov, A., W. I. Newman, and D. L. Turcotte (1999), An exactly soluble hierarchical clustering model: inverse cascades, self-similarity, and scaling, *Phys. Rev. E*, *60*, 5293-5300.

- [13] Gabrielov, A. M., I. V. Zaliapin, V. I. Keilis-Borok, and W. I. Newman (2000b), Colliding Cascades as a Model for Earthquake Prediction, *Geophys. J. Int.*, *143*, 427-437.
- [14] Ghil, M., I. Zaliapin, and B. Coluzzi (2008), Boolean Delay Equations: A Simple Way of Looking at Complex Systems. *Physica D*, *237*, 2967-2986.
- [15] Guzzetti, F., C. P. Stark, and P. Salvati (2005), Evaluation of flood and landslide risk to the population of Italy, *Environmental Management*, *36*(1), 1536.
- [16] Hara, T. and G. Slade (1990), Mean-field critical behaviour for percolation in high dimensions. *Commun. Math. Phys.*, *128*, 333-391.
- [17] Horton, R. E. (1945), Erosional development of streams and their drainage basins: Hydrophysical approach to quantitative morphology, *Geol. Soc. Am. Bull.*, *56*, 275-370.
- [18] Keilis-Borok, V., J. H. Stock, A. Soloviev, and P. Mikhalev (2000), Pre-recession pattern of six economic indicators in the USA, *J. Forecasting*, *19*, 65-80.
- [19] Keilis-Borok, V. I. and A. A. Soloviev (eds.) (2003), *Nonlinear Dynamics of the Lithosphere and Earthquake Prediction*, Springer-Verlag, Heidelberg, 337 pp.
- [20] Lashermes, B., E. Foufoula-Georgiou, and W. E. Dietrich (2007), Channel network extraction from high resolution topography using wavelets, *Geophys. Res. Lett.*, *34*, L23S04, doi:10.1029/2007GL031140.
- [21] Leyvraz, F. (2003), Scaling theory and exactly solved models in the kinetics of irreversible aggregation, *Phys. Rep.*, *383*(2-3), 95-212.
- [22] Maher, B. A. (2002), Uprooting the Tree of Life, *The Scientist*, *16*: 18.
- [23] Mandelbrot, B. B. (1983), *The Fractal Geometry of Nature*, W. H. Freeman, New York.
- [24] Marani, A., R. Rigon, and A. Rinaldo (1991), A note on fractal channel networks, *Water Resour. Res.*, *27*(12), 3041-3049.
- [25] McConnell, M., and V. Gupta (2008), A proof of the Horton law of stream numbers for the Tokunaga model of river networks. *Fractals*, *16*(3), 227-233.

- [26] Morein, G., W. I. Newman, D. L. Turcotte, and A. M. Gabrielov (2005), An inverse cascade model for self-organized complexity and natural hazards, *Geophys. J. Int.*, *163*, 433-442.
- [27] Molchan, G., O. Dmitrieva, I. Rotwain and J. Dewey (1990), Statistical analysis of the results of earthquake prediction, based on bursts of aftershocks, *Phys. Earth Planet. Inter.*, *61*, 128-139.
- [28] Narkunskaya, G. S. and M. G. Shnirman (1990), Hierarchical model of defect development and seismicity, *Phys. Earth. Planet. Inter.*, *61*, 29-35.
- [29] Newman, W. I. and A. M. Gabrielov (1991), Failure of hierarchical distributions of fiber bundles. I, *Internat. J. of Fracture*, *50*, 1-14.
- [30] Newman, W. I., D. L. Turcotte, and A. M. Gabrielov (1997), Fractal trees with side branching, *Fractals*, *5*, 603-614.
- [31] Newman, W. I., D. L. Turcotte, and A. M. Gabrielov (1995), Log-periodic behavior of a hierarchical failure model with applications to precursory seismic activation, *Phys. Rev. E*, *52*, 4827-4835.
- [32] Peckham, S. (1995), New results for self-similar trees with applications to river networks, *Water Resour. Res.*, *31(4)*, 1023-1029.
- [33] Passalacqua, P., T. Tang, E. Foufoula-Georgiou, G. Sapiro, and W. E. Dietrich (2009) River network extraction from high-resolution topography: Nonlinear diffusion and geodesic paths, *Water Resour. Res.*, in review.
- [34] Peckham, S. and V. Gupta (1999), A reformulation of Horton's laws for large river networks in terms of statistical self-similarity, *Water Resour. Res.*, *35(9)*, 2763-2777.
- [35] Pelletier, J. D. and D. L. Turcotte (2000), Shapes of river networks and leaves: Are they statistically similar? *Phil. Trans. R. Soc. London, B(355)*, 307-311.
- [36] Pinna, M., A. Fonnesu, F. Sangiorgio, and A. Basset (2004), Influence of summer drought on spatial patterns of resource availability and detritus processing in Mediterranean stream sub-basins (Sardinia, Italy), *Internat. Rev. Hydrobiol.*, *89(5-6)*, 484-499.
- [37] Rammal, R., G. Toulouse, and M. A. Virasoro (1986) Ultrametricity for physicists, *Rev. Mod. Phys.*, *58*, 765-788.

- [38] Rodriguez-Iturbe, I. and A. Rinaldo (1997), *Fractal River Networks: Chance and Self-Organization*, Cambridge University Press, New York.
- [39] Rodriguez-Iturbe, I., E. Ijjasz-Vasquez, R. L. Bras, and D. G. Tarboton (1992), Power law distributions of mass and energy in river basins, *Water Resour. Res.*, *28(4)*, 10891093.
- [40] Rotwain, I., V. Keilis-Borok, and L. Botvina (1997), Premonitory transformation of steel fracturing and seismicity, *Phys. Earth Planet. Inter.*, *101*, 61-71.
- [41] Schikhof, W. H. (2007), *Ultrametric Calculus: An Introduction to P-Adic Analysis*, Cambridge University Press, New York, 318 pp.
- [42] Shnirman, M. G., E. M. Blanter (2001), Criticality in a dynamic mixed system. *Phys. Rev. E*, *64(5)*, No. 056123, Part 2.
- [43] Shreve, R. L. (1966), Statistical law of stream numbers. *J. Geol.*, *74*, 17-37.
- [44] Sklar L. S., W. E. Dietrich, E. Foufoula-Georgiou, B. Lashermes, D. Bellugi (2006), Do gravel bed river size distributions record channel network structure?, *Water Resour. Res.*, *42*, W06D18, doi:10.1029/2006WR005035.
- [45] Sinai, Ya. G. (1974), Construction of Cluster Dynamics for Dynamical Systems of Statistical Mechanics, *Proc. of Moscow State University*, *1*, 152.
- [46] Sinai, Ya. G. (1973), Constuction of Dynmaics in Infinite Systems of Particles, *Theoretical and Mathematical Physics*, *12*, 487.
- [47] Sposito, G. (ed.) (1998), *Scale Dependence and Scale Invariance in Hydrology*, Cambridge Univ. Press, New York.
- [48] Stauffer, D. and A. Aharony (1994), *Introduction to Percolation Theory*, 2-nd ed., Taylor & Francis.
- [49] Strahler, A. N. (1957), Quantitative analysis of watershed geomorphology, *Trans. Am. Geophys. Un.*, *38*, 913-920.
- [50] Tokunaga, E. (1978), Consideration on the composition of drainage networks and their evolution, *Geographical Rep. Tokyo Metro. Univ.*, *13*, 1-27.

- [51] Turcotte, D. L. (1997), *Fractals and Chaos in Geology and Geophysics*, 2-nd ed, Cambridge University Press, 398 pp.
- [52] Turcotte, D. L., B. D. Malamud, G. Morein, and W. I. Newman (1999), An inverse cascade model for self-organized critical behavior, *Physica A*, *268*, 629-643.
- [53] Turcotte, D. L., B. D. Malamud, F. Guzzetti, and P. Reichenbach (2002), Self-organization, the cascade model, and natural hazards, *Proc. Natl. Ac. Sci.*, *99*, 2530-2537.
- [54] Turcotte, D. L., J. D. Pelletier, and W. I. Newman (1998), Networks with side branching in biology. *J. Theor. Biology*, *193(4)*, 577-592.
- [55] Zaliapin, I. (2009), Horton laws in self-similar trees. Manuscript.
- [56] Zaliapin, I., V. Keilis-Borok, and M. Ghil (2003), A Boolean Delay Model of Colliding Cascades. II: Prediction of Critical Transitions, *J. Stat. Phys.*, *111(3-4)*, 839-861.
- [57] Zaliapin, I., H. Wong, and A. Gabrielov (2005), Inverse cascade in percolation model: Hierarchical description of time-dependent scaling, *Phys. Rev. E*, *71*, No. 066118.

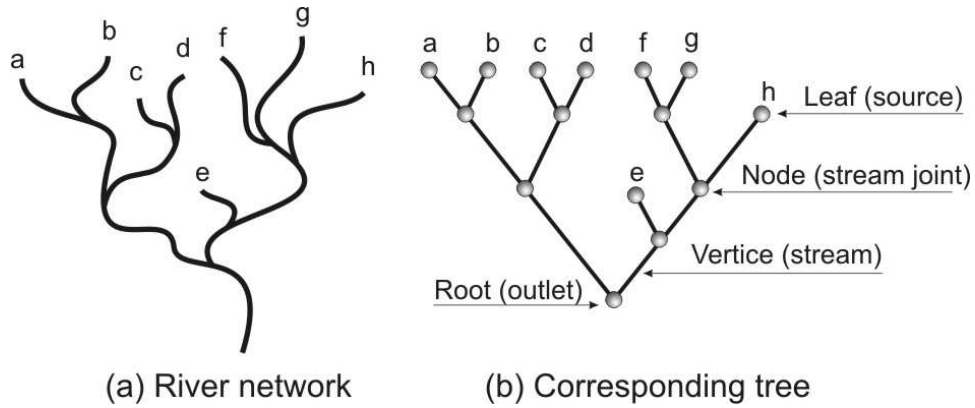


Figure 1: Tree representation of a river network: (a) hypothetical river network; and (b) its representation by a binary tree. The network sources and the respective tree leaves are marked by the same letters in both panels. The figure also illustrates the terminology used in our river transport study.

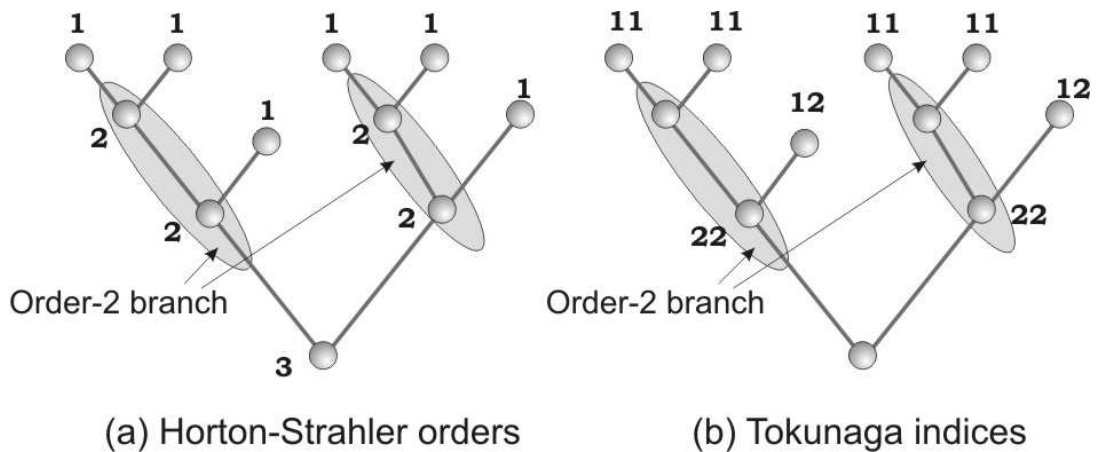


Figure 2: Example of (a) Horton-Strahler ordering, and (b) Tokunaga indexing.

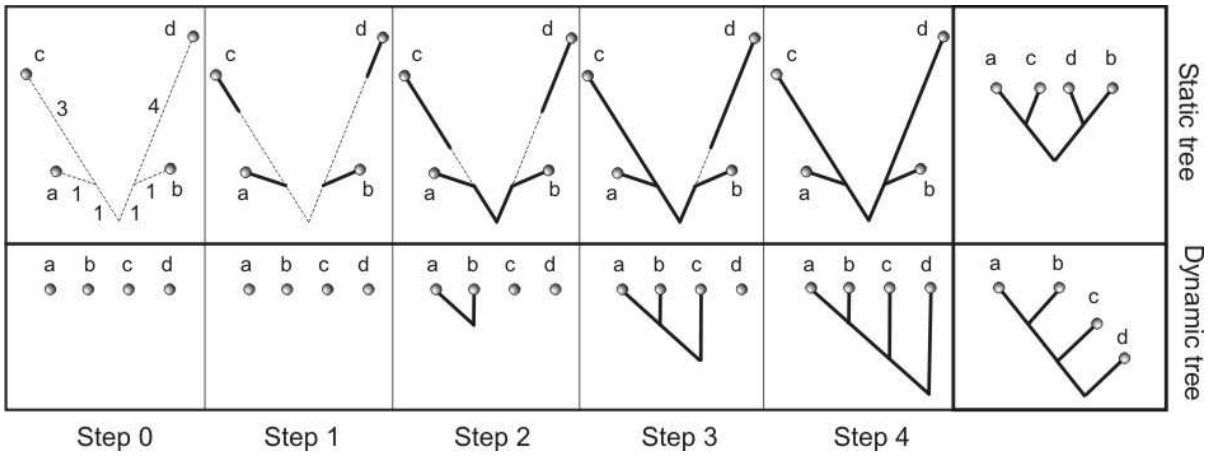


Figure 3: Constructing a *dynamic* tree. The initial static tree and the final dynamic tree are shown in the rightmost pair of panels. The dynamic tree reflects the propagation of a flux from leaves to the root of the static tree at a constant velocity. The top row of panels shows the static tree at different steps of this process; for visual convenience we explicitly show the static tree's link lengths. The bottom row shows the corresponding phases of the dynamic tree. The top leftmost panel indicates the lengths of the links in the static tree; each step in the figure takes one time unit, that is the flux propagates one unit of length downstream. See Section 3.1 for details.

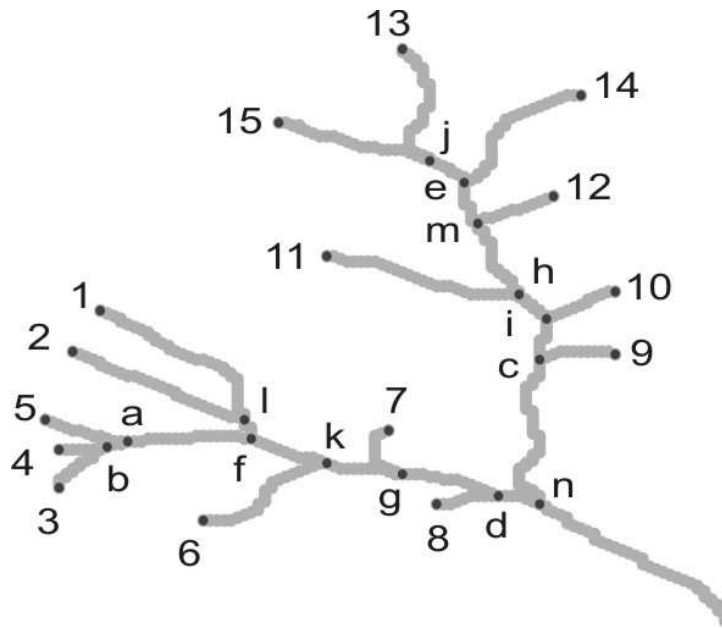


Figure 4: Stream network for an order-3 subbasin of the Noyo river basin, Mendocino county, California. Sources are marked by letters, stream merging points by numbers. The same marks are used in Figs. 5 and 6 that show the static and dynamic trees for this stream.

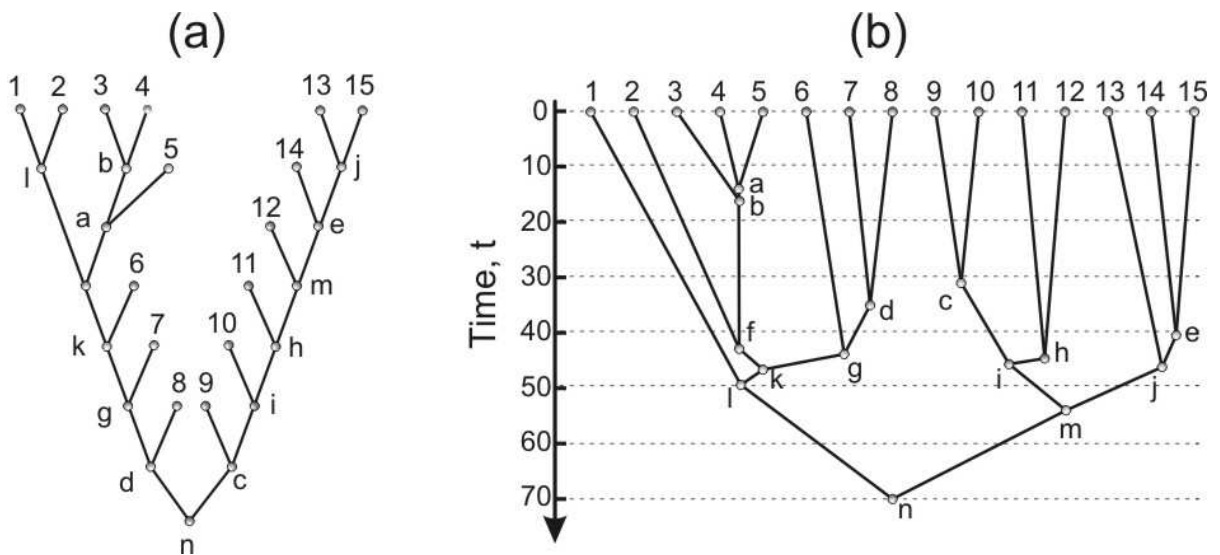


Figure 5: Static and dynamic trees for the Noyo subbasin of Fig. 4. (a) Static tree T_S and (b) dynamic tree T_D . Letter and number marks are the same as in Fig. 4.

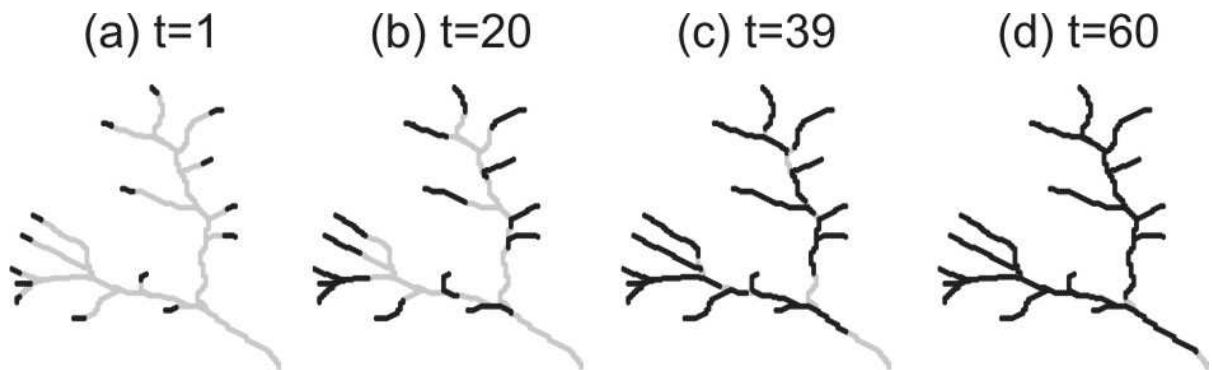


Figure 6: Three snapshots of the evolution of the dynamic tree (heavy solid lines) on the static tree (light solid lines) for the stream of Fig. 4. Letter and number marks are the same as in Fig. 4.

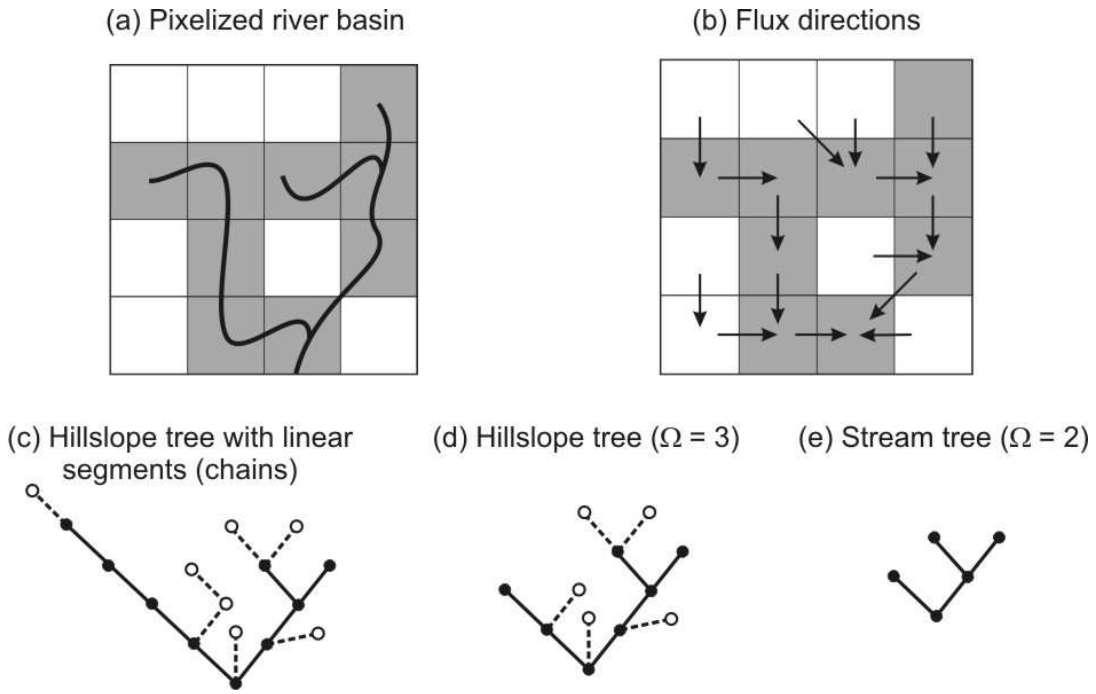


Figure 7: Construction of a *static* tree that represents the topology of hillslope (unchannelized) and stream (channelized) drainage paths. (a) Pixelized river basin; the shaded pixels (cells) correspond to the stream location (solid line), the white pixels – to the valleys or hillslopes. (b) Flux direction obtained from the elevation data. (c) Tree that describes the drainage topology: solid nodes and links correspond to the stream pixels and stream flow; open nodes and dashed links – to the hillslope pixels and hillslope flow. Notice that this tree contains several purely linear segments, with no branching. (d) The same tree, from which the linear segments have been removed: it describes the topology of both hillslope paths and stream paths, and is referred to as the *hillslope tree*. (e) The subset of the tree in panel (d) that describes the topology of the stream paths only; this tree is referred to as the *stream tree*.

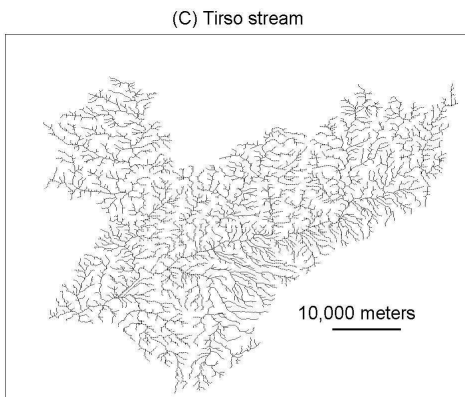
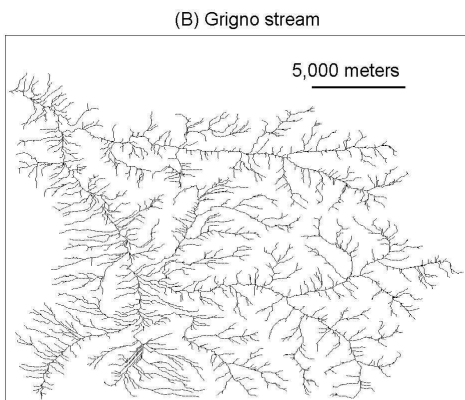
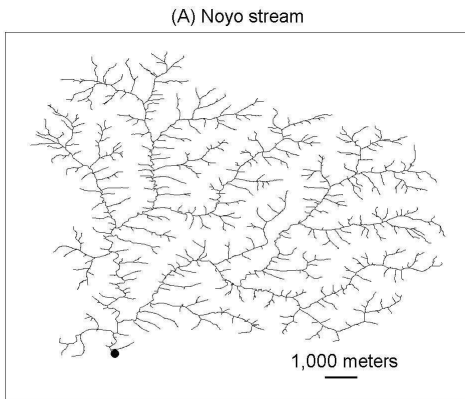


Figure 8: Static trees for the stream networks of the three basins analyzed in this study. a) Noyo, Mendocino County, California, USA; the outlet is marked by a ball; b) Grigno, Trento, Italy; c) Tirso, Sardinia, Italy. See Section 6.1 for details of channel initiation.

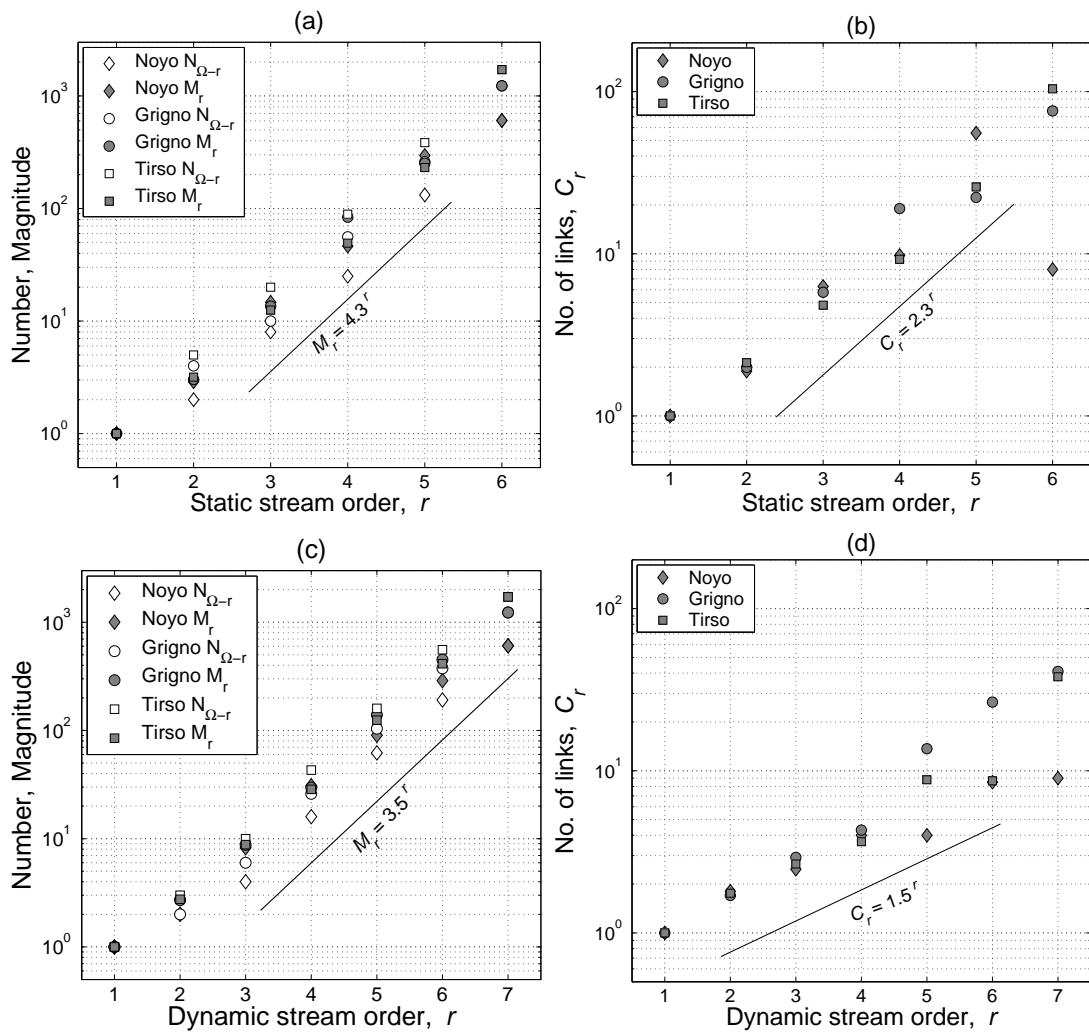


Figure 9: Branching statistics for the stream trees of Noyo, Grigno, and Tirso basins. Number N_r and average magnitude M_r for static (panel a) and dynamic (panel c) trees and average number C_r of links within a branch for static (panel b) and dynamic (panel d) trees.

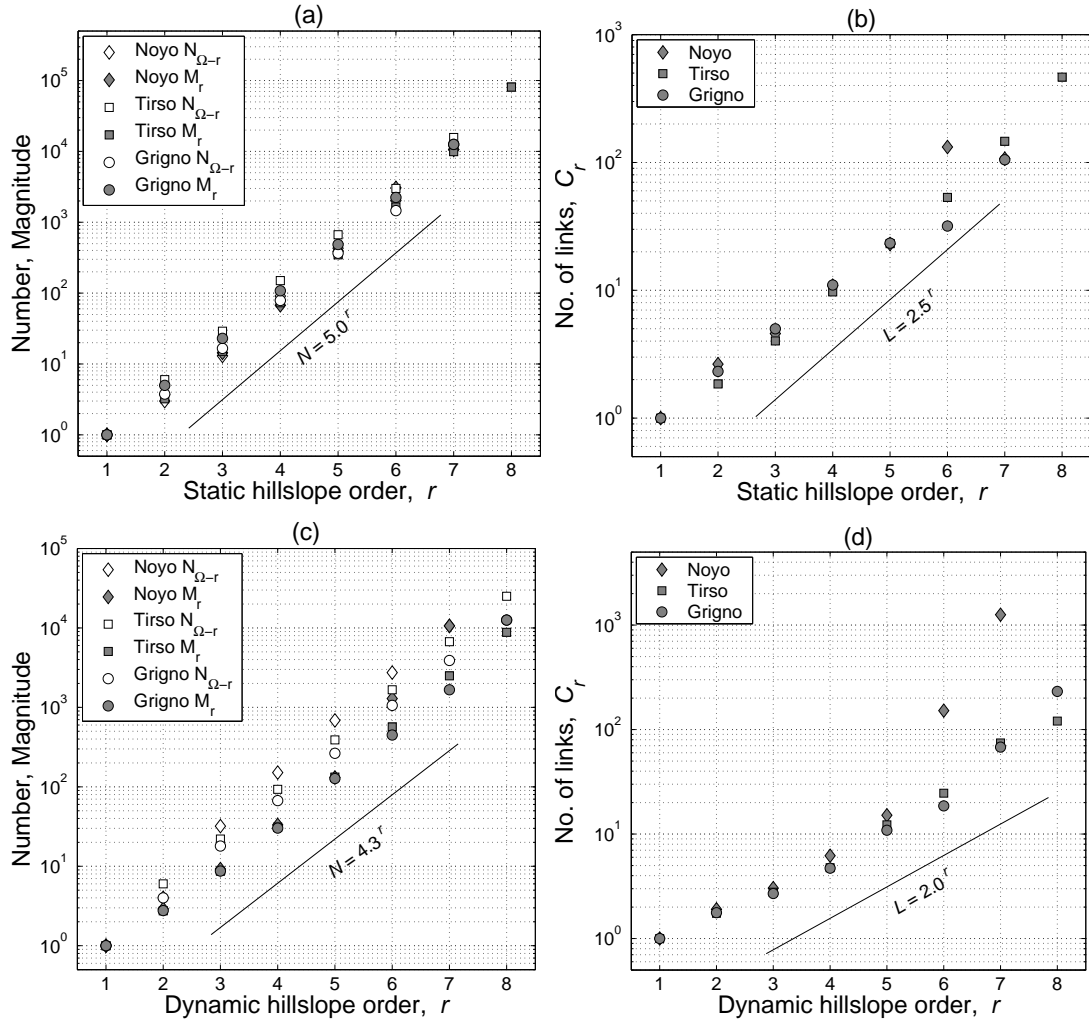


Figure 10: Branching statistics for the hillslope trees of Noyo, Grigno, and Tirso basins. Number N_r and average magnitude M_r for static (panel a) and dynamic (panel c) trees and average number C_r of links within a branch for static (panel b) and dynamic (panel d) trees.

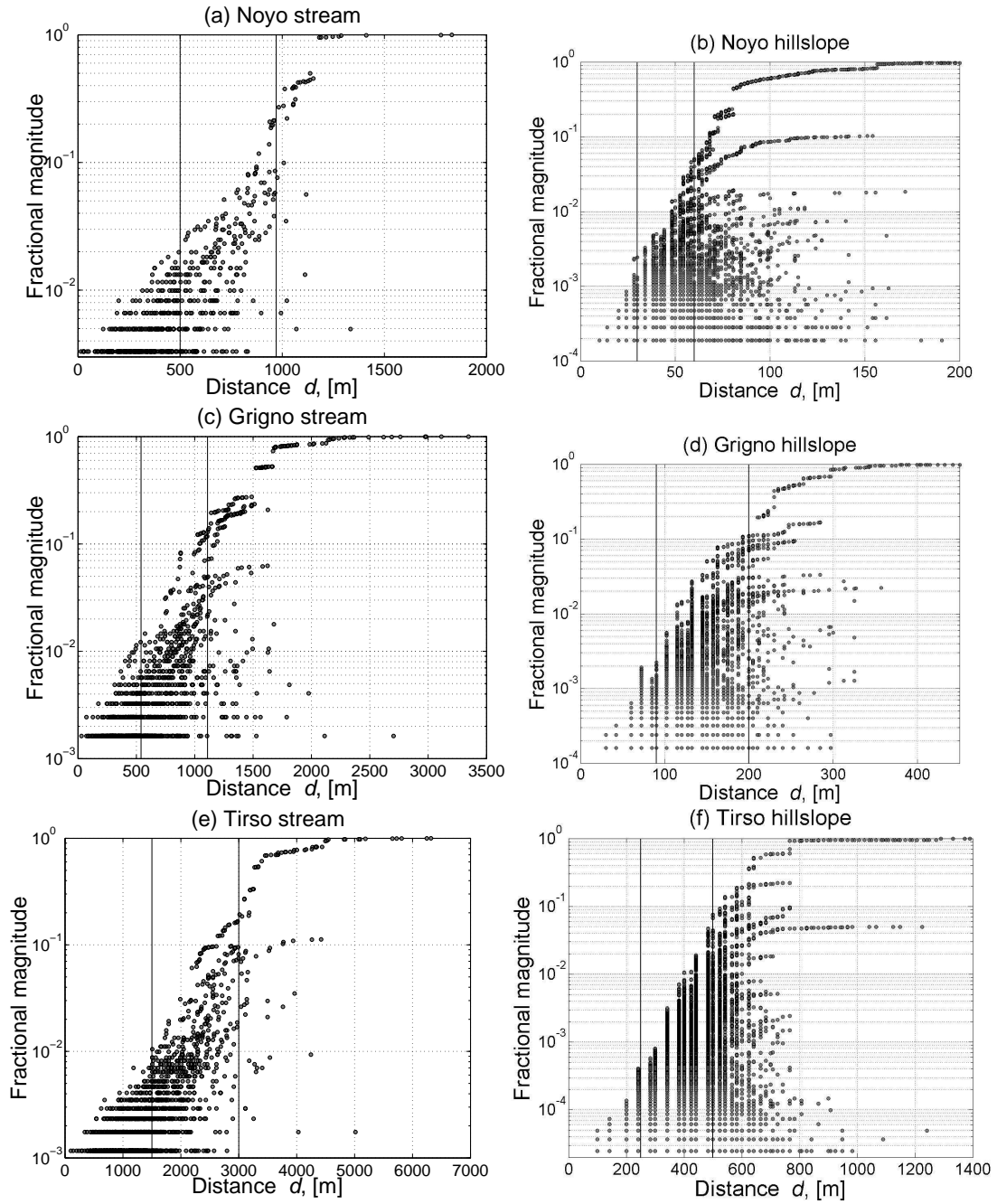


Figure 11: Fractional branch magnitudes m_i/N as a function of the distance d_i traveled by the dye at the branch creation instant. Notice that the distance d_i can be interpreted as the time t_i necessary to create the branch. a) Noyo stream; b) Noyo hillslope; c) Grigno stream; d) Grigno hillslope; e) Tirso stream; f) Tirso hillslope.

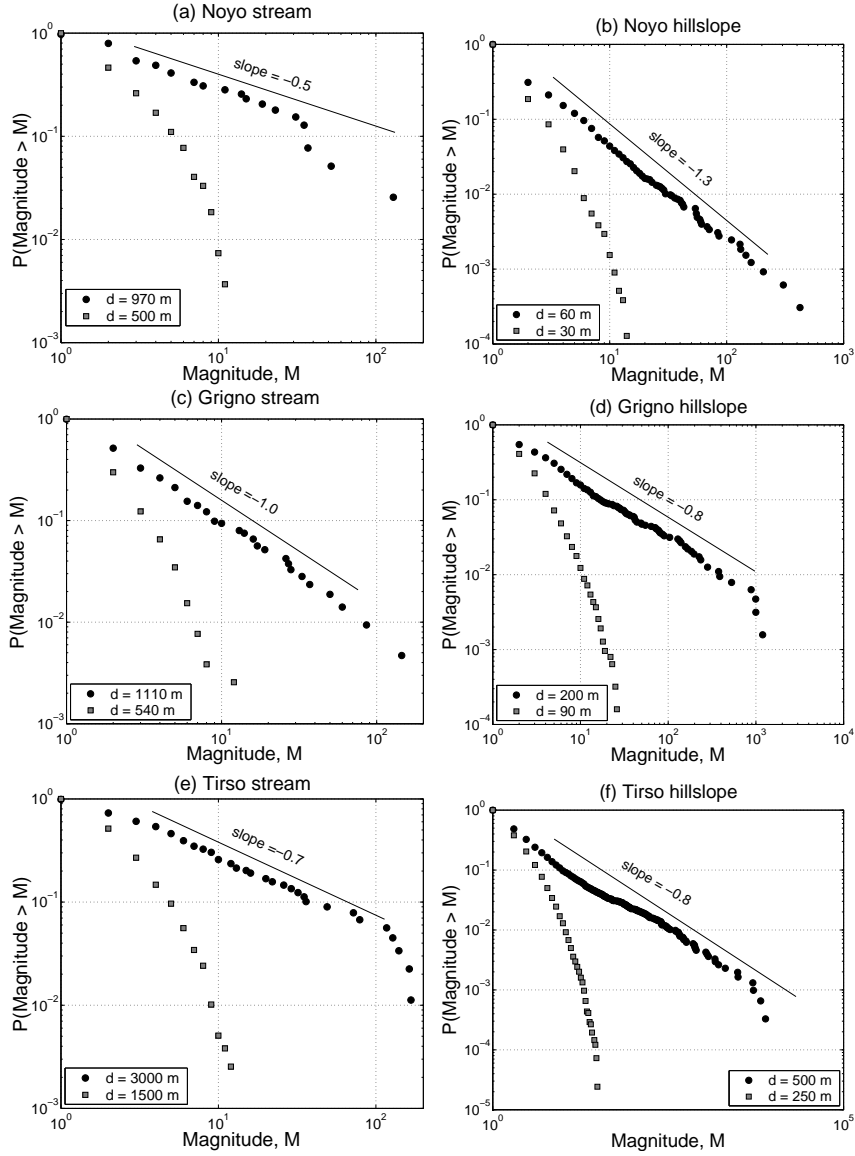


Figure 12: Distribution of branch magnitudes m_i at the critical distance d^* (balls) and at an earlier time (squares) in dynamic trees for the three basins. a) Noyo stream; b) Noyo hillslope; c) Grigno stream; d) Grigno hillslope; e) Tirso stream; f) Tirso hillslope. Each panel shows two distributions, the corresponding distances are depicted by vertical lines in Fig. 11. Notice that the value of the critical distance d^* can be interpreted as the critical time t^* necessary to create the critical cluster. The downward deviations from the pure power laws are due to the finite-size effect.

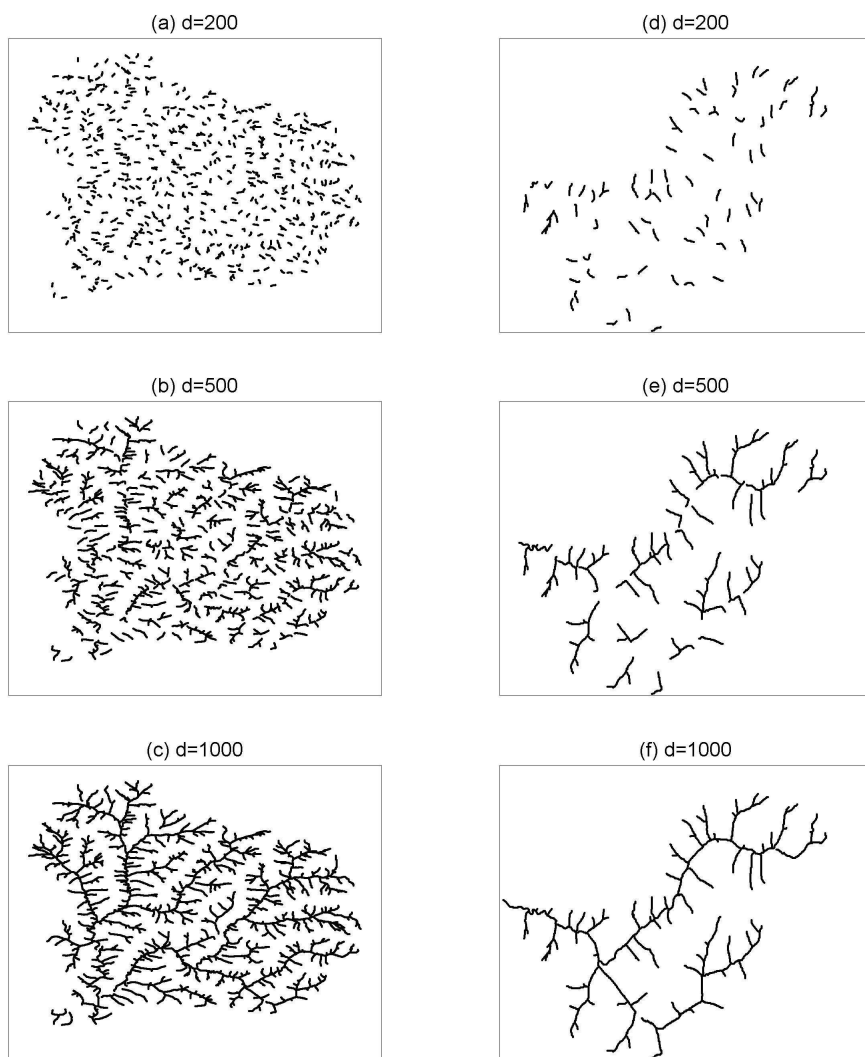


Figure 13: Transport down the Noyo stream network. Three snapshots of flux propagation from the stream sources to the outlet, at (a,d) $d = 200$, (b,e) $d = 500$, and (c,f) $d = 1000$. Panels (a)–(c) show the entire Noyo basin, while panels (d)–(f) zoom onto an order-4 subbasin located in the lower right part of the entire basin. See also Fig. 14.

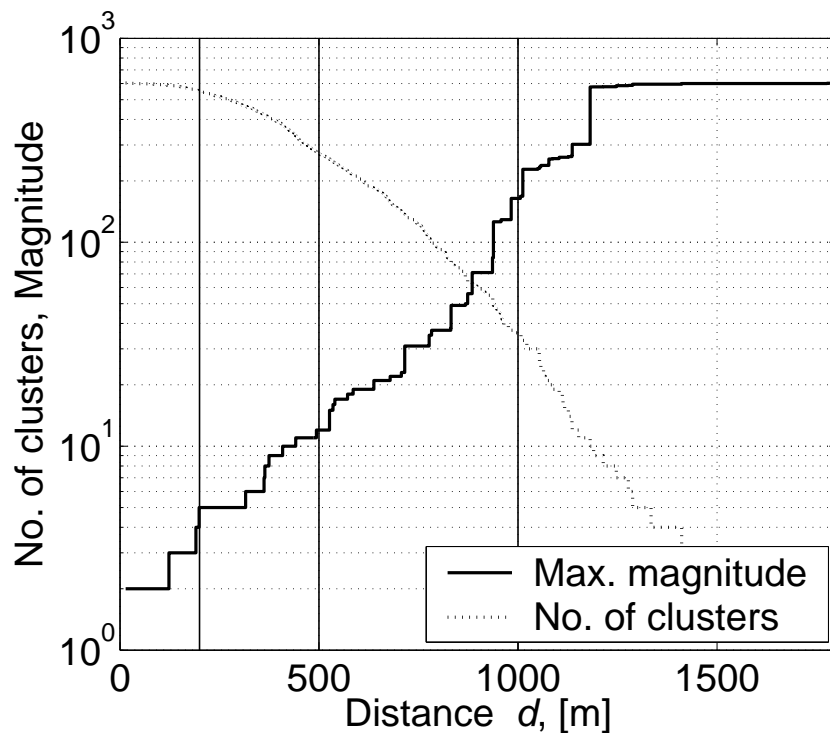


Figure 14: Cluster evolution for the Noyo downstream flux transport: number (dotted line) and largest-cluster size (solid line). Vertical lines correspond to the three snapshots in Fig. 13.

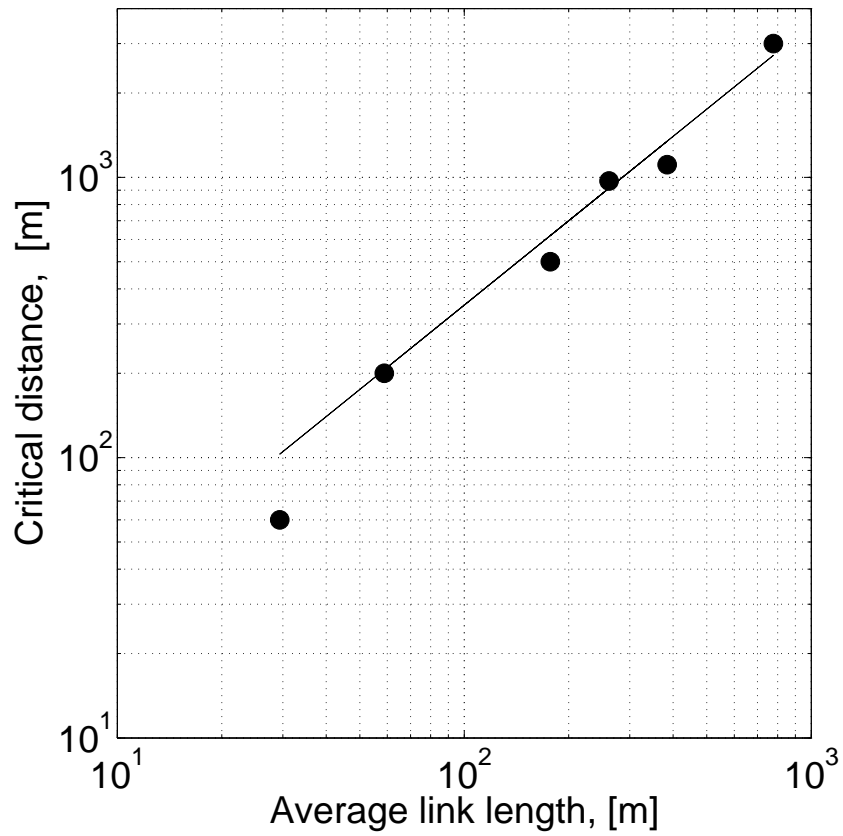


Figure 15: Critical distance d^* as a function of the average link length \bar{L} for the six dynamic trees shown in Fig. 11. The line in the figure corresponds to $d^* = 3.5 \bar{L}$.